Science Arts & Métiers (SAM)
is an open access repository that collects the work of Arts et Métiers Institute of Technology researchers and makes it freely available over the web where possible.

This is an author-deposited version published in: https://sam.ensam.eu
Handle ID: .http://hdl.handle.net/10985/23053

To cite this version :

Ravi Raj Purohit PURUSHOTTAM RAJ PUROHIT, Daniel Pepin FOWAN, Elsa THUNE, Stephan ARNAUD, Gilbert CHAHINE, Nils BLANC, René GUINEBRETIÈRE, Olivier CASTELNAU - Phase transition and twinning in polycrystals probed by in situ high temperature 3D reciprocal space mapping - Applied Physical Letters - Vol. 121, n°18, p.181901 - 2022

Any correspondence concerning this service should be sent to the repository Administrator : scienceouverte@ensam.eu

Phase transition and twinning in polycrystals probed by *in situ* high temperature 3D reciprocal space mapping

Ravi Raj Purohit Purushottam Raj Purohit,[1] Daniel Pepin Fowan,[2] Elsa Thune,[2] Stephan Arnaud,[3] Gilbert Chahine,[4] Nils Blanc,[3] Olivier Castelnau,[5] and René Guinebretière[2,a)]

AFFILIATIONS

[1]Université Grenoble Alpes, CEA, IRIG, MEM, CNRS, 17 Avenue des Martyrs, Grenoble 38000, France
[2]Université de Limoges, IRCER, UMR CNRS 7315, 12 rue Atlantis, 87068 Limoges, France
[3]Université Grenoble Alpes, CNRS, Institut Néel UPR CNRS 2940, 38000 Grenoble, France
[4]SIMaP, Grenoble INP, CNRS, Université Grenoble Alpes, 38000 Grenoble, France
[5]Laboratoire PIMM, UMR CNRS 8006, ENSAM, CNAM, 151 Bd de l'Hôpital, 75013 Paris, France

[a)]**Author to whom correspondence should be addressed:** rene.guinebretiere@unilimfr.fr

ABSTRACT

Polycrystalline materials exhibit physical properties that are driven by both the interatomic crystallographic structure as well as the nature and density of structural defects. Crystallographic evolutions driven by phase transitions and associated twinning process can be observed *in situ* in three-dimensional (3D) using monochromatic synchrotron radiation at very high temperatures (over 1000 °C). This paper focuses on continuous measurements of the 3D-reciprocal space maps by high-resolution x-ray diffraction as a function of temperature along a phase transition process occurring between 1200 °C and room temperature. These high precision measurements allow observing the reciprocal space node splitting and the evolution of the diffuse scattering signal around that node as a function of temperature. The capability of this experimental method is illustrated by direct *in situ* high temperature measurements of the 3D splitting of a reciprocal space node due to phase transition recorded on dense pure zirconia polycrystals.

Solid-state phase transitions (SPTs) are fundamental processes that drive large part of the effective physical properties of single crystals as well as polycrystalline materials. Aside from the structural evolutions that can be described with respect to space group transitions,[1] the SPTs are very often associated with transformations that occur on the mesoscale and that generate structural defects like dislocations, twinning, stacking faults, etc.,[2] and associated strain fields. Over the years, the study of such imperfect crystals has driven the development of direct space imaging methods used to observe defects at convenient scale down to the nanometer range. Apart from electronic microscopy, which remains essentially a destructive experimental approach, nondestructive methods based on x-ray absorption or scattering have become more common. High-resolution x-ray computed tomography using a synchrotron radiation source reaches a spatial resolution below hundred nanometers,[3] and Bragg coherent x-ray diffraction imaging allows visualizing structural defects in sub-micrometric crystals.[4] Moreover, both of these methods are now used for *in situ* measurements under different types of external constrains.[5,6]

As an alternative to imaging in the direct space, defects can also be observed and quantitatively studied in the reciprocal space through high-resolution x-ray diffraction experiments without the use of any complex phase-retrieval algorithm. The reciprocal space mapping (RSM) method, originally developed for the study of defects in epitaxial layers,[7] has been extended to many cases ranging from imperfect single crystals[8] to complex polycrystals.[9] Over the recent decade, the widespread use of 2D solid state detectors at synchrotron beamlines has facilitated the development of three-dimensional (3D)-RSM on timescale that enables one to follow the sample evolutions as a function of external stimuli.[10,11] In the case of polycrystals, it has been shown that this approach allows, in reciprocal space, the selection of the crystals of interest in the probed volume.[12] We have recently demonstrated that this method can be used even at very high temperatures.[13,14]

This paper aims to extend the 3D-RSM method to the *in situ* observations of solid-state phase transitions that occur in polycrystals at high temperatures. The potential of this approach is illustrated by examining two successive phase transitions in dense polycrystals of pure zirconia. In this paper, we demonstrate that the method permits following the temperature induced splitting of an initially unique reciprocal lattice node (RLN) into 24 RLNs, which results from the loss of the symmetry axis through two successive phase transitions. The quality of the 3D-data allows us to fully index these 24 RLNs.

Due to the ability of zirconium to accommodate different atomic coordinations, pure zirconia (ZrO_2) crystallizes in different phases depending on pressure and temperature. At atmospheric pressure, pure, unstressed zirconia solidifies into a cubic crystal structure (*c*—space group $Fm\bar{3}m$) at about 2700 °C, transforms to a tetragonal structure (*t*—space group $P4_2/nmc$) when cooled to 2300 °C, and to a monoclinic structure (*m*—space group $P2_1/c$) at 1170 °C.[15] To describe these two SPTs, we refer to the initial crystallographic axis of the parent cubic crystal. Accordingly, as it is often done (see, for example, Ref. 16), the structure of tetragonal zirconia is indexed in a pseudo-cubic "face-centered tetragonal" lattice, where the $\vec{a}_t$, $\vec{b}_t$, and $\vec{c}_t$ unit cell vectors of the tetragonal lattice are co-linear to the cubic unit cell vectors $\vec{a}_c$, $\vec{b}_c$, and $\vec{c}_c$.

The description of the true crystallographic path between the pure cubic and monoclinic phases of zirconia remains much debated. The $P4_2/nmc$ space group is a sub-group of $Fm\bar{3}m$, and the $c \longrightarrow t$ transition is generally considered as a second order phase transition.[15,17] The crystallographic description of the $t \leftrightarrow m$ SPT is more complex.[18] In the pure zirconia single crystal, it is a first-order one and is associated with a strong volume variation. It has been shown that an intermediate orthorhombic phase can be identified,[15,19] and it has been experimentally observed in polycrystalline doped zirconia materials[20] and nanosized pure zirconia crystals without external stress[21] as well as under stresses.[22] However, it is unclear whether the orthorhombic phase is an intermediate state between the *t* and *m* phases or whether it is an alternative to the *m* phase.[19,23] The complete description of the phase transition of pure zirconia is beyond the scope of this paper; however, we will show that this phase transition can be followed *in situ* by recording the 3D distribution of the x-ray diffracted intensity in the reciprocal space as a function of temperature. Throughout this paper, we will illustrate the above-mentioned phase transitions by the *in situ* observation of the high temperature splitting of the 111 cubic RLN.

During the cooling process from the liquid state, the first SPT corresponds to the transition between the $m\,\bar{3}\,m$ and the $4/m\ m\ m$ point groups. Accordingly, the threefold $\langle 111 \rangle$ cubic symmetry axis is lost through this $c \longrightarrow t$ SPT. As illustrated in Fig. 1(a), this results in three equivalent 111 tetragonal spots in the reciprocal space. The $t \longrightarrow m$ SPT promotes the transition between the $4/m\ m\ m$ and the $2/m$ point groups. Therefore, it corresponds to the loss of two mirrors and the transition from a fourfold to twofold axis. This corresponds to $2 \times 2 \times 2 = 8$ possibilities, i.e., eight crystallographic variants. Considering the respective crystal lattice orientation among *c*, *t*, and *m* phases[25] and the lattice parameters of each phase,[14] one can easily compute the coordinate of all RLNs in the reciprocal space, taking here Q_x, Q_y, and Q_z parallel to the axes of the parent cubic lattice. This is illustrated for one of the tetragonal variants, and the locations of the eight associated monoclinic RLNs generated by the $t \longrightarrow m$ SPT are reported in Fig. 1(b). Finally, considering the two phase transitions, we get $3 \times 8 = 24$ monoclinic variants.[24,25] In the monoclinic state, the 111 and $\bar{1}11$ RLNs are not equivalent, and the respective norm of the reciprocal lattice vectors *Q* differs. Consequently, the monoclinic nodes are distributed in two subsets, each with 12 monoclinic RLNs, located either above (larger *Q* value) or below (smaller *Q* value) the three 111_t nodes [see Fig. 1(c)]. For each of the Q vector norm, the 12 monoclinic RLNs are distributed into three subsets, each containing four nodes. Finally, the diffracted intensities of monoclinic crystals are distributed in six distinct parts of the reciprocal space, each containing four monoclinic nodes [see Fig. 1(c)], and they are located in three groups either above or below the parent cubic 111 RLN. The exact positions of the three tetragonal and 24 monoclinic RLNs depend on the cell parameter values at the temperature under consideration. All along this paper, these values are extracted from the thermal expansion laws established in Ref. 14 and reported in Table I. Because the $t \longrightarrow m$ SPT is considered here, only the laws determined for the cooling process are useful. (Coefficients for heating have been found to differ slightly.[14])

From the experimental point of view, the best way to illustrate the relationships between twin crystals resulting from the phase transition process of a parent crystal is to find a situation where both phases exist under given external conditions. In such a case, the phase transition can be directly observed by *in situ* experiments in the appropriate region of the reciprocal space. Nevertheless, such a goal requires using a polycrystalline sample containing a portion of the crystals in a metastable state. In the present case, we have used dense bulk samples of pure zirconia obtained from large sub-meter refractory blocks

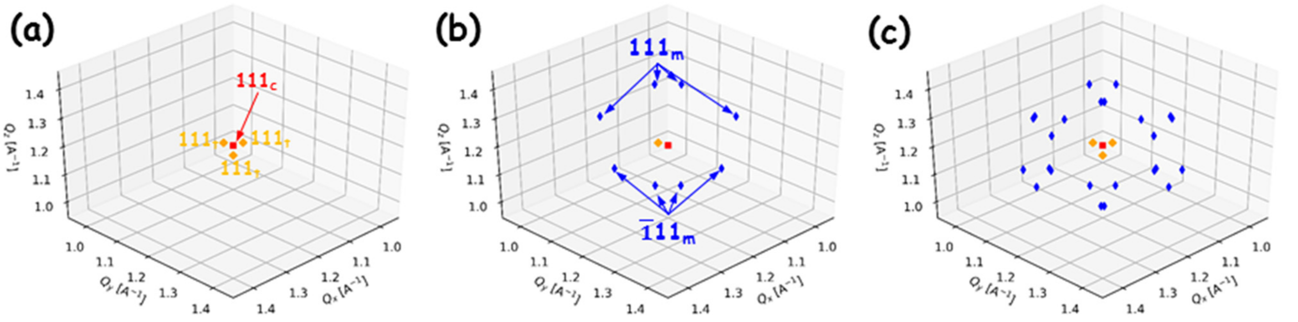

FIG. 1. Splitting of the cubic zirconia 111 node (red square) through the $c \longrightarrow t$ and $t \longrightarrow m$ SPTs. (a) splitting of the 111_c node into three 111_t nodes (orange diamonds) through the $c \longrightarrow t$ SPT. (b) Splitting of one of the 111_t nodes into eight monoclinic nodes (blue diamonds), four 111_m nodes and four $\bar{1}11_m$ nodes. (c) Assuming the presence of the three tetragonal variants, 24 monoclinic nodes are presents. The positions of all the nodes are calculated here for a temperature of 950 °C during the cooling process, according to the cell parameters indicated in Table I.

TABLE I. Linear evolution of the monoclinic and tetragonal pure zirconia cell parameters as a function of temperature (°C) during cooling.[14]

Zirconia phases	Cell parameters	Thermal expansion laws (°C)
m-ZrO_2	a_m (nm)	$0.515 + 4.54 \times 10^{-6}$ T
	b_m (nm)	$0.520 + 1.55 \times 10^{-6}$ T
	c_m (nm)	$0.534 + 5.66 \times 10^{-6}$ T
	β_m (deg)	$99.5 - 7.86 \times 10^{-4}$ T
t-ZrO_2	a_t (nm)	$0.509 + 4.89 \times 10^{-6}$ T
	c_t (nm)	$0.521 + 5.69 \times 10^{-6}$ T

fuse-casted by the Saint-Gobain company. After cooling, the material consists in large areas of pure zirconia embedded in silica-based glass. These sub-millimeter volume regions contain a very large number of nanometer-sized crystals[14,26,27] (e.g., see the TEM images shown Fig. 1[14,27]). A full description of the relationship between the elaboration process and the microstructure of this material has been reported elsewhere.[26]

All 3D-RSMs were recorded at the French CRG beamline D2AM installed at the ESRF (Grenoble, France). The layout and the capabilities of this beamline for such measurements have been described elsewhere.[28] A 2D-detector (ImXPAD D5 Hybrid pixel detector, 560 × 960 pixels, pixel size 130 μm) was used, the energy of the x-ray beam was fixed at 17.5 keV, and the distance between the sample and the detector was ~0.80 m. In this configuration, 2D slices of the reciprocal space can be recorded with convenient resolution without movements of the detector. The full measurement of one 3D-RSM was done by combining 600 2D-slices (ω scans with 0.02° step), and this took around 45 min. We have used the QMAX furnace[13] that was mounted on top of a motorized goniometer head (four-axes, for sample surface alignment) installed on the six-circles goniometer of the beamline. The probed volume is defined by the size of the x-ray beam, which was set to $300 \times 30\,\mu\text{m}^2$ (H × V). This corresponds approximately to a square footprint ($300 \times 300\,\mu\text{m}^2$) on the sample considering the x-ray incidence angle. Taking into account the x-ray energy, the depth of the probed volume can be estimated to be 100 μm. Accordingly, "a sample probed by x ray" (gauge volume) has a dense volume of about $9 \times 10^6\,\mu\text{m}^3$, which contains millions of nanosized crystals. Depending on the temperature and the orientation of this gauge volume relative to the goniometer axis, some monoclinic or tetragonal crystals diffract and contribute to the diffracted intensities in each 3D-RSM. Using the X–Y cross translation stages located below the goniometer head, it was possible to select without any doubt a gauge volume that was filled at high temperatures with only one unique parent cubic crystal.[14] This was possible as one knows that the cubic domains at high temperatures are well identified, surrounded by a glassy phase, and millimetric in size,[26] i.e., larger than the x-ray gauge volume.

As mentioned above, the $t \leftrightarrow m$ transition of pure and perfect zirconia crystals without any stress occurs at 1170 °C. Reheating the sample from room temperature to 1250 °C causes all the zirconia crystals to transform into their tetragonal form.[14] Cooling of the sample induces the $t \rightarrow m$ transition, but due to the presence of a high level of internal local stresses,[27] at temperatures below 1000 °C, monoclinic and tetragonal zirconia crystals coexist simultaneously, and the phase transition of all the metastable tetragonal crystals is spread within a temperature range of about one thousand degrees.[14] Such a polycrystal, which simultaneously contains two different structures of pure zirconia crystals, is, therefore, a very good sample for the detection of phase transition related twinning via *in situ* high temperature RSM. This situation is illustrated in Fig. 2(a), which has been recorded at 500 °C during cooling. The figure clearly shows the presence of monoclinic nodes around the central 111_t node. At a given temperature, the phase transition nucleates in many different parts of the transforming crystal, i.e., the two phase transition processes ($c \rightarrow t$ and $t \rightarrow m$) occur from different areas of the parent cubic crystal. Starting with a sub-millimeter cubic single crystal, this leads to the emergence of very large numbers of nanometer-sized tetragonal and monoclinic crystals.[29] During 3D reciprocal space mapping performed at a given temperature, some of these crystals are in Bragg conditions for the $\{111\}_t$, $\{111\}_m$, or $\{\bar{1}11\}_m$ planes and diffract. Therefore, the intensity distribution recorded in the 3D-RSM comes from a large number of diffracting crystals. Given the initial orientation of the cubic crystal, the orientation of each of the monoclinic nanosized crystals is one of the 24 variants indicated in Fig. 1. The calculated positions (white dots) of all the 24 monoclinic RLNs are overlaid on the RSM recorded at room temperature [Fig. 2(b)]. The splitting of the 111_t RLN depicted in Fig. 1 clearly agrees well with the location of the intensity maxima observed in the 3D-RSM reported in Fig. 2(b). The respective crystallographic orientations of two adjacent monoclinic crystals correspond to one of the possible twin relationships that arise between the two different variants. RSM imaging of the splitting around such a RLN during the temperature-induced phase transition illustrates the *in situ* twinning process.

It is worth noting that the intensity maxima observed in Figs. 2(a) and 2(b) are accompanied by a significant diffuse scattering signal that is distributed over a large portion of the mapped reciprocal space volume. Part of this diffuse scattering signal is certainly related to thermal vibration of the atoms [the so-called thermal diffuse scattering (TDS) signal]. Nevertheless, the temperature under consideration here is quite low with respect to the liquidus pure zirconia temperature, and the contribution of TDS cannot explain such a high level of the diffuse scattering signal. We already demonstrated[27] that the studied pure zirconia crystals are subjected to huge stresses (GPa range) generated by the SPTs, which induces a large amount of elastic strains. The presence of the diffuse scattering signal may be related to the presence of this strain field. As preliminary results, we report in Fig. 2(d) the 1D-intensity distributions extracted from the RSM recorded at room temperature, linking monoclinic RLNs in pairs at opposite positions relative to the tetragonal 111 RLN [see Fig. 2(c)]. The cylinders are drawn so that they all pass through the common center of the 111_t cloud, and the angle among cylinders 1, 2, and 3 is each 120° (from the loss of the threefold symmetry axis). The 1D intensity distribution [Fig. 2(d)] presents broad and intense diffuse scattering signals superimposed to the observed diffraction maxima. Given that the crystals considered are pure zirconia, no compositional fluctuation is possible. Consequently, this diffuse scattering signal is probably associated with a continuous change in the d-spacing that is directly linked to elastic strains. The evolution of this signal as a function of temperature is not the subject of this work and will be discussed in a forthcoming article.

In situ observations of $c \rightarrow t$ SPT in the pure zirconia polycrystal are very challenging given the temperatures required for such observations and have never been performed to the authors' knowledge.

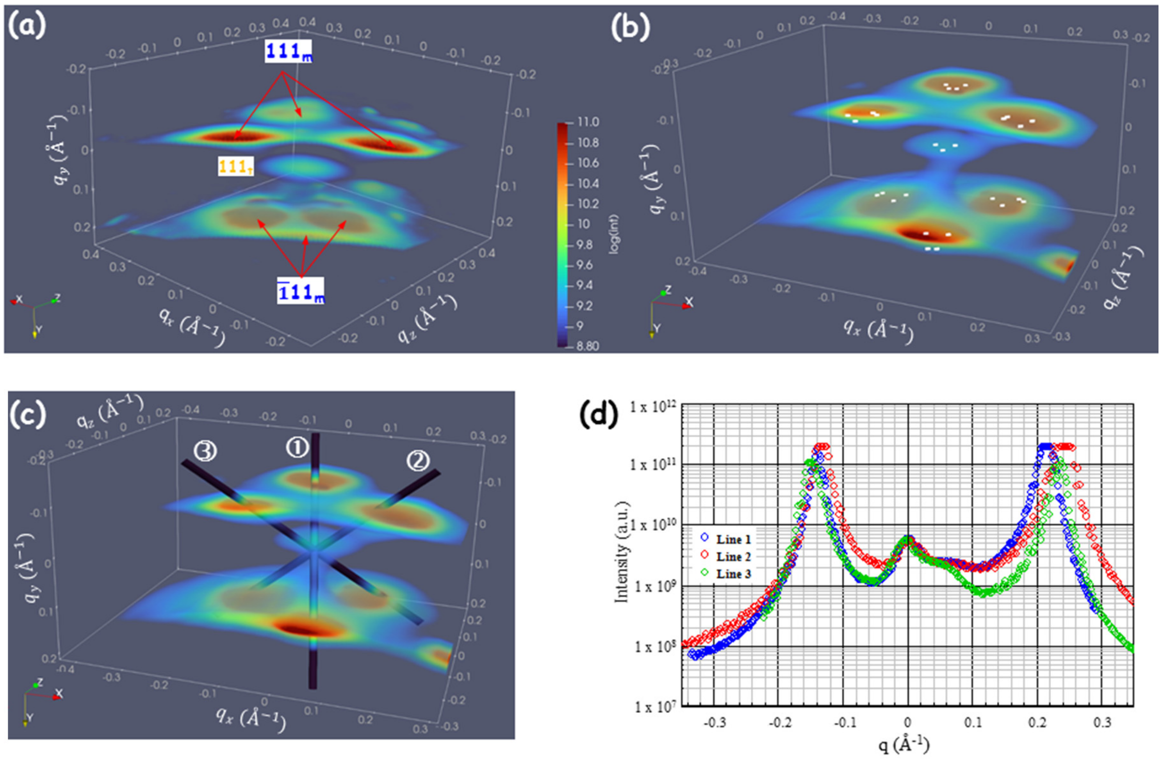

FIG. 2. RSMs recorded near the pure zirconia 111_t node, demonstrating the simultaneous presence of both tetragonal and monoclinic crystals generated through phase transition processes occurring in one unique cubic crystal during cooling from 1250 °C. (a) RSM recorded at 500 °C. The intensity maxima observed above and below the 111_t node are due to the diffraction of monoclinic crystals. (b) RSM recorded at room temperature including the calculated positions of the 24 expected monoclinic RLNs (white dots). (c) Representation of cylindrical extractions of the diffracted and scattered signals. (d) 1D integrated intensity distributions of cylinders along the 1, 2, and 3 axes and with diameter 0.01 Å^{-1}.

Nevertheless, as shown in Fig. 1(a), this SPT results in the formation of three 111_t RLNs near the initial 111_c node. As mentioned before, all the crystals in the gauge volume that were examined come from a single cubic parent crystal. Accordingly, a reciprocal space map around the calculated position of the 111_c RLN at a given temperature must allow for the observation of this threefold cubic axis splitting. The 3D-RSM recorded at 1150 °C (Fig. 3) illustrates the $c \rightarrow t$ transition that occurs during cooling, where all zirconia crystals are in the tetragonal form. From the value of the cell parameters at this temperature,[14] the theoretical positions of the three 111_t nodes can be calculated. These positions

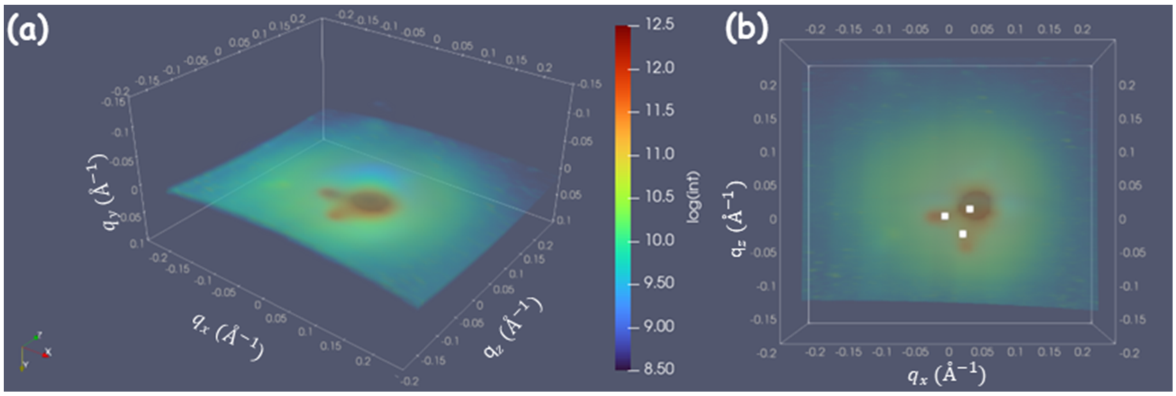

FIG. 3. Threefold splitting of the 111_c node through the $c \rightarrow t$ SPT. RSM recorded *in situ* at 1150 °C and theoretical positions of the 111_t RLNs [white dots superimposed to the top view in (b)] at this temperature.

are superimposed on the experimental 3D-RSM shown in Fig. 3 and qualitatively match the locations of the three measured diffraction intensity maxima.

The setup described above allows following the $t \rightarrow$ m SPT during cooling in fine temperature steps (here, 5 °C). The complete 3D-RSM reconstruction of the evolution of the diffraction signal with temperature is presented as a video in the supplementary material. Some representative maps are reported in Fig. 4. Lowering the temperature from 990 to 980 °C causes a significant portion of the tetragonal crystals to transform into monoclinic. We have verified that the measured positions of the intensity maxima in the RSMs agree well with theoretical positions, as already shown in Fig. 2(b). Below 980 °C, the presence of both tetragonal and monoclinic zirconia crystals can be clearly observed. One can also observe specific features at 975 and 970 °C with significantly more spots in the RSM than at higher and lower temperatures. This behavior is related to the complexity of the $t \rightarrow$ m phase transition process, possibly linked to the existence of an intermediate orthorhombic state. More generally, it could also be due to the preeminence of some of the 24 variants with respect to the others. While a full discussion of this is beyond the scope of this paper, observations like this illustrate the effectiveness of 3D reciprocal space mapping at high temperatures in capturing fine structural evolutions. As illustrated in Fig. 4, despite the high temperature, the evolution of the 3D-RSM was followed continuously, implying that the probed

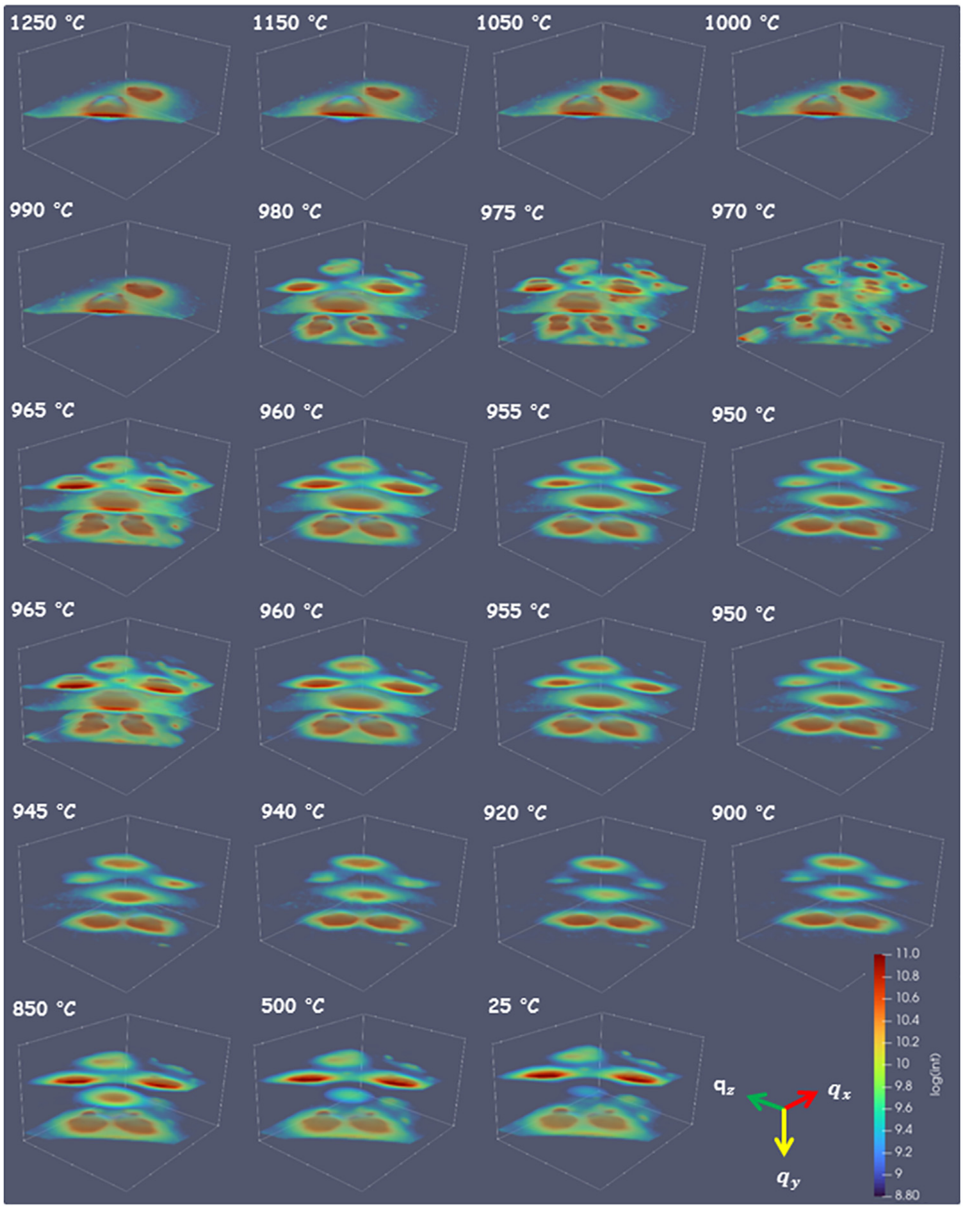

FIG. 4. *In situ* high-temperature observation of the splitting of the tetragonal 111 RLN during the tetragonal to monoclinic phase transition in pure zirconia. q_x is between −0.2 and 0.2; q_y is also between −0.2 and 0.2; while q_z is between −0.2 and 0.3. Image etiquettes (tick marks along the axis) are every 0.1 Å.

volume remains in the same position relative to the incoming x-ray beam and all the parts of the goniometer. As anticipated from Fig. 4, the evolution of the 3D-RSM between 500 °C and room temperature (not shown here) is smooth and related to the conventional cell parameters' thermal evolutions.

It is well-known that measuring the diffuse scattering signal near or far from the Bragg peak is a method of choice for studying phase transition processes in single crystals.[30] The case of polycrystals is more complex, but it is of particular interest since most of the materials used in the industry are polycrystalline. It has been demonstrated here that the mapping of the reciprocal space associated with the diffraction by a polycrystal can be performed on a timescale well-suited for the *in situ* probing of temperature-induced phase transitions. In the field of applied condensed matter, samples are usually composed of large number of three-dimensional crystals. Therefore, the associated reciprocal space is also three-dimensional. Any crystallographic phenomenon that occurs during phase transitions is necessarily associated with some evolutions of at least one feature of the 3D-RSM recorded in the vicinity of the crystals RLNs, and the signature of such phase transitions can be observed by the experimental method detailed in this work. Finally, as an *in situ* method, it, in principle, allows one to capture any intermediate crystallographic state that may arise during the phase transition processes.

See the supplementary material for video observation of the splitting of the 111 RLN as a function of the temperature recorded between 1250 °C and room temperature.

This work was performed within the framework of the HoTMiX Research Program co-funded by the ANR (No. ANR-19-CE09-0035) and DFG. We acknowledge the ESRF and the French Collaborating Research Group (F-CRG) for the provision of the synchrotron radiation facilities beamtimes. The authors are thankful to I. Cabodi and O. Bories (Saint-Gobain CREE) for the supply of the bulk zirconia-based materials.

AUTHOR DECLARATIONS

Conflict of Interest

The authors have no conflicts to disclose.

Author Contributions

Ravi Raj Purohit Purushottam Raj Purohit: Data curation (lead); Formal analysis (equal); Investigation (equal); Methodology (equal); Software (lead); Visualization (equal); Writing – original draft (equal); Writing – review & editing (lead). **Daniel Pepin Fowan:** Formal analysis (supporting); Investigation (equal); Methodology (equal). **Elsa Thune:** Writing – review & editing (supporting). **Stephan Arnaud:** Investigation (equal); Methodology (equal). **Gilbert André Chahine:** Data curation (equal); Formal analysis (supporting); Investigation (equal); Methodology (equal); Validation (equal); Writing – review & editing (equal). **Nils Blanc:** Conceptualization (equal); Data curation (equal); Formal analysis (equal); Investigation (equal); Methodology (equal); Software (equal); Writing – review & editing (equal). **Olivier Castelnau:** Conceptualization (equal); Data curation (equal); Formal analysis (equal); Investigation (equal); Methodology (equal); Software (equal); Supervision (equal); Validation (equal); Writing – original draft (equal); Writing – review & editing (lead). **René Guinebretière:** Conceptualization (lead); Data curation (equal); Formal analysis (lead); Funding acquisition (lead); Investigation (equal); Methodology (equal); Project administration (lead); Supervision (lead); Writing – original draft (lead); Writing – review & editing (lead).

DATA AVAILABILITY

The data that support the findings of this study are available from the corresponding author upon reasonable request.

REFERENCES

[1] U. Müller, *Symmetry Relationships Between Crystal Structures* (Oxford University Press, 2013).

[2] A. P. Levanyuk and A. S. Sigov, *Defects and Structural Phase Transitions* (Gordon and Breach Science Publishers, 1988).

[3] R. Mokso, P. Cloetens, E. Maire, W. Ludwig, and J. Y. Buffière, "Nanoscale zoom tomography with hard x rays using Kirkpatrick-Baez optics," Appl. Phys. Lett. **90**, 144104 (2007).

[4] M. A. Pfeifer, G. J. Williams, I. A. Vartanyants, R. Harder, and I. K. Robinson, "Three-dimensional mapping of a deformation field inside a nanocrystal," Nature **442**, 63–66 (2006).

[5] J. Villanova, R. Daudin, P. Lhuissier, D. Jauffrès, S. Lou, C. L. Martin, S. Labouré, R. Tucoulou, G. Martinez-Criado, and L. Salvo, "Fast *in situ* 3D nanoimaging: A new tool for dynamic characterization in materials science," Mater. Today **20**, 354–359 (2017).

[6] J. Shin, T. W. Cornelius, S. Labat, F. Lauraux, M. I. Richard, G. Richter, N. P. Blanchard, D. S. Gianolac, and O. Thomas, "*In situ* Bragg coherent x-ray diffraction during tensile testing of an individual Au nanowire," J. Appl. Crystallogr. **51**, 781–788 (2018).

[7] P. F. Fewster, "Reciprocal space mapping," Crit. Rev. Solid State Mater. Sci. **22**, 69–110 (1997).

[8] A. Boulle, D. Chaussende, L. Latu-Romain, F. Conchon, O. Masson, and R. Guinebretière, "X-ray diffuse scattering from stacking faults in thick 3C-Si C single crystals," Appl. Phys. Lett. **89**, 091902 (2006).

[9] E. Filippelli, G. Chahine, and A. Borbely, "Evaluation of intragranular strain and average dislocation density in single grains of a polycrystal using K-map scanning," J. Appl. Crystallogr. **49**, 1814–1817 (2016).

[10] B. Croes, F. Cheynis, Y. Zhang, C. Voulot, K. D. Dorkenoo, S. Chrifi-Hertel, C. Mocuta, M. Texier, T. W. Cornelius, O. Thomas, M. I. Richard, P. Muller, S. Curiotto, and F. Leroy, "Ferroelectric nanodomains in epitaxial GeTe thin films," Phys. Rev. Mater. **5**, 124415 (2021).

[11] S. P. Zeuschner, M. Mattern, J. E. Pudell, A. von Reppert, M. Rössle, W. Leitenberger, J. Schwarzkopf, J. E. Boschker, M. Herzog, and M. Bargheer, "Reciprocal space slicing: A time-efficient approach to femtosecond x-ray diffraction," Struct. Dyn. **8**, 014302 (2021).

[12] H. Palancher, P. Goudeau, A. Boulle, F. Rieutord, V. Favre-Nicolin, N. Blanc, G. Martin, J. Fouet, and C. Onofri, "Strain profiles in ion implanted ceramic polycrystals: An approach based on reciprocal-space crystal selection," Appl. Phys. Lett. **108**, 031903 (2016).

[13] R. Guinebretière, S. Arnaud, N. Blanc, N. Boudet, E. Thune, D. Babonneau, and O. Castelnau, "Full reciprocal-space mapping up to 2000 K under controlled atmosphere: The multipurpose QMAX furnace," J. Appl. Crystallogr. **53**, 650–661 (2020).

[14] R. Guinebretière, T. Ors, V. Michel, E. Thune, M. Huger, S. Arnaud, N. Blanc, N. Boudet, and O. Castelnau, "Coupling between elastic strains and phase transition in dense pure zirconia polycrystals," Phys. Rev. Mater. **6**, 013602 (2022).

[15] M. Smirnov, A. Mirgorodsky, and R. Guinebretière, "Phenomenological theory of lattice dynamics and polymorphism of ZrO_2," Phys. Rev. B **68**, 104106 (2003).

[16] E. Kisi, *Zirconia Engineering Ceramics: Old Challenges - New Ideas* (Trans Tech Publications, Zürich, Switzerland, 1998).

[17] K. Parlinski, Z. Q. Li, and Y. Kawazoe, "First principles determination of soft mode in cubic ZrO_2," Phys. Rev. Lett. **78**, 4063–4066 (1997).

[18] R. A. Evarestov and Y. E. Kitaev, "New insight on cubic-tetragonal-monoclinic phase transitions in ZrO2: *Ab initio* study and symmetry analysis," J. Appl. Crystallogr. **49**, 1572–1578 (2016).

[19] S. H. Guan, X. J. Zhang, and Z. P. Liu, "Energy landscape of zirconia phase transitions," J. Am. Chem. Soc. **137**, 8010–8013 (2015).

[20] R. Guinebretière, Z. Oudjedi, and A. Dauger, "Orthorhombic zirconia phase in ZrO_2-$MgAl_2O_4$ composite materials," Scr. Mater. **34**, 1039–1044 (1996).

[21] S. Liu, W. Hu, Y. Zhang, J. Xiang, F. Web, B. Xu, J. He, D. Yu, Y. Tian, and Z. Liu, "Metastable adaptative orthorhombic martensite in zirconia nanoparticles," J. Appl. Cryst. **47**, 684–691 (2014).

[22] R. Guinebretière, Z. Oudjedi, B. Soulestin, and A. Dauger, "Semi-coherent zirconia inclusions in a ceramic matrix," J. Mater. Res. **15**, 2482–2487 (2000).

[23] G. Fadda, L. Truskinovsky, and G. Zanzotto, "Unified Laudau description of the tetragonal, orthorhombic and monoclinic phases of zirconia," Phys. Rev. B **66**, 174107 (2002).

[24] M. Hayakawa, N. Kuntani, and M. Oka, "Structural study on the tetragonal to monoclinic transformation in arc-melted ZrO_2-2mol.% Y_2O_3—I. Experimental observations," Acta Metall. **37**, 2223–2228 (1989).

[25] M. Humbert, N. Gey, C. Patapy, E. Joussein, M. Huger, R. Guinebretière, T. Chotard, and A. Hazotte, "Identification and orientation determination of parent cubic domains from EBSD maps of monoclinic pure zirconia," Scr. Mater. **63**, 411–414 (2010).

[26] C. Patapy, M. Huger, T. Chotard, R. Guinebretiere, N. Gey, A. Hazotte, and M. Humbert, "Solidification structure in pure zirconia liquid molten phase," J. Eur. Ceram. Soc. **33**, 259–268 (2013).

[27] T. Ors, F. Gouraud, V. Michel, M. Huger, N. Gey, J. S. Micha, O. Castelnau, and R. Guinebretière, "Huge local elastic strains in bulk nanostructured pure zirconia materials," Mater. Sci. Eng. A **806**, 140817 (2021).

[28] G. A. Chahine, N. Blanc, S. Arnaud, F. de Geuser, R. Guinebretière, and N. Boudet, "Advanced non-destructive in situ characterization of metals with the French Collaborating Research Group D2AM/BM02 beamline at the European Synchrotron Radiation Facility," Metals **9**, 352 (2019).

[29] M. Mamivand, M. A. Zaeem, H. EL Kadiri, and L. Q. Chen, "Phase field modeling of the tetragonal-to-monoclinic phase transformation in zirconia," Acta Mater. **61**, 5223 (2013).

[30] T. R. Welberry, *Diffuse X-Ray Scattering and Models of Disorder* (Oxford University Press, 2004).